Combined Action of Plasma-driven Co-generated Hydrated Electrons and Sulfate Radicals for mineralization via Reduction/Oxidation of Perfluoroalkyl Substances (PFAS)

Andressa Mota-Lima [1], Julio Romano Meneghini[1] and Claudio A. Oller do Nascimento[1]

[1] *Departamento de Engenharia Química, Escola Politécnica, Universidade de São Paulo, Av. Prof. Luciano Gualberto 380, São Paulo – SP 05508-010, Brasil.*

(Received: 24. May 2026, Accepted: 04. Nov. 2026, Published online: 16. Nov. 2026)

Plasma water treatment, has in recent years, demonstrated superior performed compared with other technologies in its ability to abate perfluoroalkyl substances (PFAS) in aqueous matrices. Recent computational experiments using Chemical Reaction Network (CRN) modeling (*J. Technol. Space Plasmas*, vol. 6, no. 1, pp. 202–217, May 2025, doi: 10.31281/vab52w73) suggest that plasma-phase H• radical are the direct cause of PFAS reduction and abatement when employing an electrified plasma/liquid interface (EPLI). However, this hypothesis has not yet been experimentally validated. The same study demonstrates that EPLI-induced hydrated electrons (e_{aq}^-) reduce PFAS with poor extension (low Faradaic efficiency), owing to the relatively low PFOA concentration. In the present contribution, CRN computational experiments were performed to demonstrate how EPLI-induced e_{aq}^- can activate $SO_4^{\bullet-}$ radicals, enabling the in-situ generation of additional reactive species rather than allowing e_{aq}^- to reduce water. The CRN computational results demonstrate that the combined action of e_{aq}^- and $SO_4^{\bullet-}$radicals offer an effective strategy for PFAS mineralization (conversion into CO_2, meaning a depletion of the total organic carbon - TOC). Without optimizations, PFAS mineralization and abatement reached 13% due to the action of $SO_4^{\bullet-}$ and 90% due to the action of e_{aq}^-, respectively, when considering 5 mM of $S_2O_8^-$ and 8mA. To the best of our knowledge, this is the first proposal to exploit EPLI-induced hydrated electrons to activate $SO_4^{\bullet-}$ radicals for PFAS mineralization, although experimental validation at the bench scale remains necessary.

DOI: https://doi.org/10.31281/d9q7p823

mota@usp.br

I. Introduction

Plasma water treatment has demonstrated to be capable of abating perfluoroalkyl substances (PFAS) in water matrix with better energy performance than other technologies. [1-6] A discharge over the liquid surface creates the electrified plasma/liquid interface (EPLI) known for simultaneously production of both the hydrated electrons (e_{aq}^-) in the aqueous phase [7] and other radicals in the plasma-phase. The spectrum of plasma-phase radicals, however, rely on the nature of the discharging gases. If humidified, any noble gas (Helium and Argon) can produce O, OH and H radicals. [8] Among these plasma radicals, H-radical has been suggested to be the key species driving PFAS abatement at plasma/liquid interface, even in the presence of other reductive species within the aqueous phase, such as EPLI-induced hydrated electrons and aqueous H-radical. [9] In view of these previous findings, [9] we foresee the use of EPLI-induced hydrated electrons to activate sulfate radical ($SO_4^{\bullet-}$), which are oxidative radicals with the potential to further degrade PFAS to completion (mineralization), rather than solely degrading them through an initial reduction step driven by other radicals. In our analysis, the sulphate radicals can assist the full oxidation (mineralization) of PFAS, as they may act complementarily to the earlier stage of PFAS abatement driven by either e_{aq}^- or H-radical reduction.

Fig. 1 depicts the current understanding of the mechanism believed to explain the outperformance of PFAS degradation with EPLI-based technology. A representative of the PFAS

 © by the author(s) 202X, Layout by G-Labs

pollutant, Perfluorooctanoic Acid (PFOA, $C_8HF_{15}O_2$) is directly reduced by e_{aq}^- produzing flurite anion. [10]

$$e_{aq}^- + C_8HF_{15}O_2 \xrightarrow{k1} C_8F_{14}O_2^{\bullet} + F^- + H^+ \quad (1)$$

However, the PFAS reduction by e_{aq}^- exhibits low Faradaic efficiency, mainly due to the low PFAS concentration in the aqueous phase, [9] meaning that majority of EPLI-induced e_{aq}^- participates in competing reaction, the principal one being the water reduction.

$$2e_{aq}^- + H_2O \rightarrow H_2 + 2OH^- \quad (2)$$

Parallel to the water reduction, EPLI-induced e_{aq}^- participates on the activation of radicals such as sulfate ($SO_4^{\bullet-}$) and hydrogen ($H^{\bullet}$) [11] when in presence of ${S_2O_8}^{2-}$ and H^+ ions, respectively.

$$e_{aq}^- + H_{aq}^+ \rightarrow H^{\bullet}{}_{aq} \quad (3)$$

$$e_{aq}^- + {S_2O_8}^{2-} \rightarrow SO_4^{\bullet-} + {SO_4}^{2-} \quad (4)$$

Previous computational experiments based on Chemical Reaction Network (CRN) suggested that plasma-phase H-radical are direct cause of PFAS abatement when employing EPLI technology, a hypothesis that has not yet been experimentally validated. [9] Herein, we overlook the contribution of the plasma-phase radicals and concentrate in the EPLI-reactor. Ordinarily, sodium persulphate ($Na_2S_2O_8$) has been widely used as a precursor of the $SO_4^{\bullet-}$ radical, being converted into this species through processes referred to as activation. Several activation methods for generating radical $SO_4^{\bullet-}$has been reported, including thermal activation above 50°C, [12] which exhibits one of the best PFAS degradation performances among chemical processes, [13] alkaline activation at pH values above 10, and activation using metallic ions such as Fe^{2+}. In this work, technological use of EPLI-induced e_{aq}^- to activate radical $SO_4^{\bullet-}$ (cf. reaction in Equ. 4) is proposed and evaluated, to the best of our knowledge, for the first time.

Conventional pollutants oxidation by $SO_4^{\bullet-}$ reports rate constants of ~10^4 M^{-1} s^{-1} for short chain perfluorinated carboxylic acid [14] and of ~10^6 M^{-1} s^{-1} for polyfluoroalkyl ether acids. [15]. Departing from this information set, this work could adopt two strategies. First, PFAS fragments degradation to either carboxylic or ether acids could be implemented as routes of degradation. However, they are overlooked in the CRN currently proposed in this work. Instead, this work evaluates the PFAS reduction only, but in presence of $SO_4^{\bullet-}$activation. The maximum values of $SO_4^{\bullet-}$concentration will be used to estimate the stoichiometric concentration of PFAS allowed to be completely oxidized (mineralized).

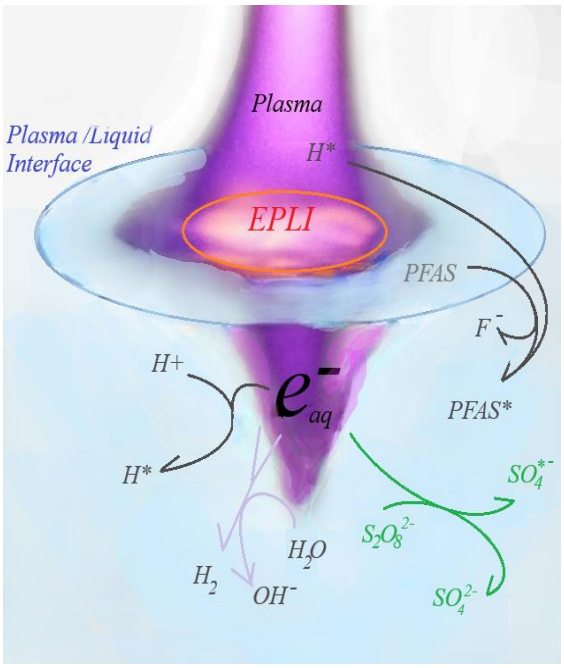


Figure 1. Current understanding of the PFAS degradation mechanism in EPLI-induced technologies. [9] Reaction highlighted in green is proposed in this contribution as additional path for further PFAS degradation till completion (mineralization). EPLI = Electrified Plasma Liquid Interface.

This study proposes mechanisms for the combined action of hydrated electron and radicals in the context of PFAS degradation using EPLI-based technology. Our investigation focuses on grounding understanding of a possible PFOA full oxidation (mineralization) by EPLI-activated $SO_4^{\bullet-}$, meaning it is inherently activated by EPLI-induced e_{aq}^-. So that, $SO_4^{\bullet-}$ could promote full oxidation of the pollutant fragment generated after an initial PFOA reduction by either the Plasma-H radical, the aqueous-H radical or EPLI-induced e_{aq}^-. This work uncovers the impact of key operational parameters, such as the initial concentration of ${S_2O_8}^{2-}$, initial pH and plasma electrical current, on promoting the highest concentrations of both $SO_4^{\bullet-}$ and $H^{\bullet}$ radicals in the liquid phase.

 © by the author(s) 2026, Layout by G-Labs

II. Theory

II.a) Intrinsic reaction triggered by the EPLI-induced e_{aq}^- and $SO_4^{\bullet-}$ radical in water matrix

The hydrated electron (e_{aq}^-) induced by the plasma electrochemistry (cathodic discharge over water) is the central species promoting reactions in the EPLI-reactor. Equ. (1) describes the PFOA reduction by the hydrated electron (e_{aq}^-), and its values of rate constant measured by Maza et al. [10] is displayed in Table 1. Besides, e_{aq}^- engages with the water reduction, leading to the hydrogen production, cf. Equ. (2). Additionally, a second route for H_2 production is provided by the hydronium ions, cf. Equ. (5) and Equ. (6).

$$e_{aq}^- + H^{\bullet}{}_{aq} + H_2O \rightarrow H_2 + OH^- \quad (5)$$

$$2H^{\bullet}{}_{aq} \rightarrow H_2 \quad (6)$$

Two of the intrinsic reaction of the radical $SO_4^{\bullet-}$ in water matrix are its own self-recombination reaction shown in Equ. (7) (cf. reaction 1 in table 15 from Neta et al. 1988), and its self-recombination with its precursor, shown in Equ. (8). [16]

$$SO_4^{\bullet} + SO_4^{\bullet-} \rightarrow S_2O_8{}^{2-} \quad (7)$$

$$SO_4^{\bullet-} + S_2O_8{}^{2-} \rightarrow SO_4{}^{2-} + S_2O_8{}^- \quad (8)$$

Additionally, the sulfate radical oxidizes water matrix, cf. reaction in Equ. (9). Given that the rate constant of water oxidation by radical $SO_4^{\bullet-}$ ($k_9 = 6.0 \times 10^1$) is substantially lower than that for either the radical self-recombination ($k_7 = 8.1 \times 10^8$) or the radical-precursor recombination ($k_8 = 1.2 \times 10^6$) reactions, one concludes that reaction in Equ. (9) is highly unfired. Yet, it will be considered in the CRN-dynamics.

$$SO_4^{\bullet-} + H_2O \rightarrow SO_4{}^{2-} + \bullet OH + H^+ \quad (9)$$

Finally, the reaction between reactants and intermediates (any specie formed in the reaction mentioned before) are shown below.

$$S_2O_8{}^{2-} + H^{\bullet}{}_{aq} \rightarrow SO_4{}^{2-} + HSO_4{}^- \quad (10)$$

$$H^{\bullet}{}_{aq} + C_8HF_{15}O_2 \xrightarrow{k12} radical^{\bullet} + F^- \quad (11)$$

II.b) CRN mathematical model

Fig. 2 shows the Chemical reaction network (CRN) for the mechanism of PFOA degradation in presence of radical sulphate ($SO_4^{\bullet-}$) proposed in this work. This CRN were built up using the reactions from Equ. (1) to Equ. (10). The set of ordinary differential equations (ODEs) describing the linear system defined by this CRN gathers Equ. (12) to Equ. (17).

Among the parameters used in this linear system are the rate constants ($k_1$to k_{11}) whose values obtained from studies with spectroscopic dynamics are shown in table 1. There are other parameters in the ODE set, namely $V$and q_e, which represent the volume of the EPLI-reactor and rate of electron injection into it, respectively. The values assigned to V depended on the experimental set up. [17] As for q_e, it represents the time dependence of the plasma current.

In this particular ODE set, the CRN forms a linear system containing six free-variables, namely $[e]$, $[S_2O_8]$, $[R]$, [H•], [H+] and [PFOA], which respectively stands for the local concentration of hydrated electrons, sulphate radical precursor (peroxydisulfate, S_2O_8), sulphate radical ($SO_4^{\bullet-}$), hydronium radical (H•), hydrogen ion (H+), and PFOA.

In the present work, both V and q_e are assumed to be constant. The EPLI reactor, located immediately beneath the EPLI, was previously defined [17, 18]. It is an open reactor with a volume ranging from 10^{-9} to 10^{-12} L, depending primarily on the geometry of the plasma–liquid interface. A detailed estimation of the EPLI reactor volume takes into account the timescales of both chemical and diffusional processes associated with the local concentration of hydrated electrons (e_{aq}^-). [17] Table 1 reports the volume of 2.36×10^{-9} L adopted throughout this work. This value is consistent with the geometry of the plasma jet employed by well-established Brazilian researchers [18].

 © by the author(s) 2026, Layout by G-Labs

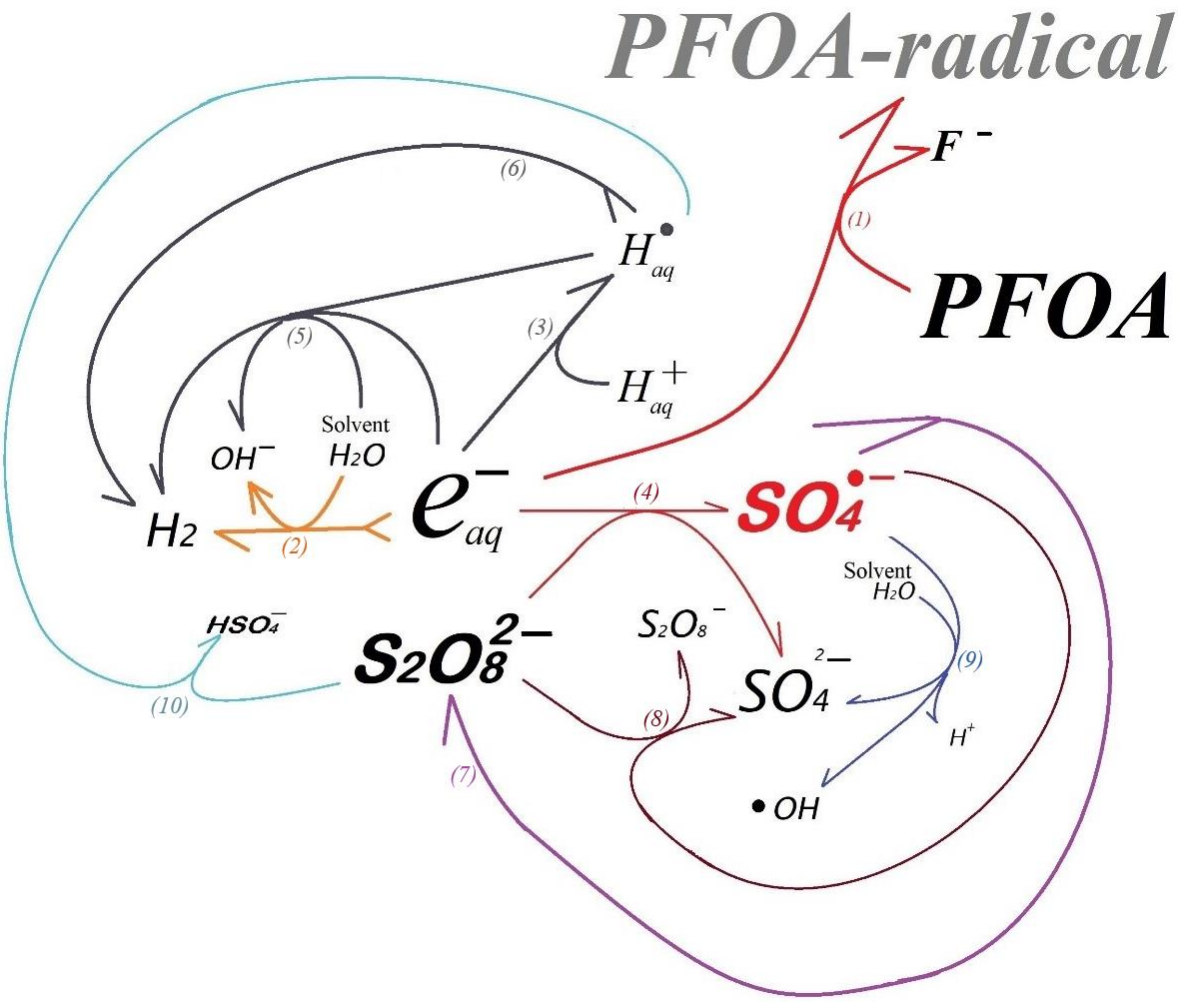


Figure 1: Chemical reaction network (CRN) for the radical $\boldsymbol{SO_4^{\bullet-}}$activation by the hydrated electrons in presence of both the PFOA and parallel reactions that scavenges the hydrated electrons producing hydrogen gas. Others: Solvent (H_2O) and H^+ are repeated in the CRN; formation of $\boldsymbol{SO_4^{\bullet-}}$ is omitted in reaction 10.

$$\frac{d[e]}{dt} = \frac{q_e}{V} - [e]\{k_1[PFOA] + 2k_2[e] + k_3[H^+] + k_4[S_2O_8] + k_5[\mathrm{H}\bullet]\} \quad (12)$$

$$\frac{d[S_2O_8]}{dt} = 2k_7[R]^2 - [S_2O_8]\{k_4[e] + k_8[R] + k_{10}[\mathrm{H}\bullet]\} \quad (13)$$

$$\frac{d[R]}{dt} = k_4[e][S_2O_8] - [R]\{2k_7[R] + k_8[S_2O_8] + k_9[R]\} \quad (14)$$

$$\frac{d[\mathrm{H}\bullet]}{dt} = k_3[\mathrm{H}^+][\mathrm{e}] - \{k_5[\mathrm{H}\bullet][e] + 2k_6[\mathrm{H}\bullet]^2 + k_{10}[\mathrm{H}\bullet][S_2O_8]\} \quad (15)$$

$$\frac{d[\mathrm{H}^+]}{dt} = -k_3[\mathrm{H}^+][\mathrm{e}] \quad (16)$$

$$\frac{d[PFOA]}{dt} = -k_1[\mathrm{PFOA}][\mathrm{e}] \quad (17)$$

Regarding the q_e parameter, it has units of mol s^{-1}, its value is estimated by considering the EPLI as an element of an electrical circuit. Since the EPLI, the plasma, and the metallic tip are all circuit elements connected in series, the same current (j) flows through all those three elements. Experimentally, the current is ordinarily measured at any point along the wires connecting the metallic tip to the high-voltage power supply. In our previous publication [17], we defined $q_e \equiv \Delta n_e/\Delta t$ as the rate at which ballistic electrons from the plasma become

 © by the author(s) 2026, Layout by G-Labs

solvated per unit time. In that work, q_e was estimated from the experimental current (j) according to:

$$q_e = \frac{j}{96485} \quad (18)$$

The electrical parameters used in our simulations are based on experimental conditions reported by Prof. Mohan Sankaran's laboratory [8], namely, a DC microplasma operating at constant current of 8 mA.

Finally, the numerical solution of the system of ordinary differential equations (ODEs), given by Equ. (12)–(17), requires the assignment of initial values to each of the six dependent variables. The initial concentrations of solvated electrons and radicals are set to zero because these species are generated locally by the electrical discharge. Thus, $[e]_0 = [R]_0 = [\mathrm{H}\bullet]_0 = zero$.

The initial pollutant concentration is assigned a value substantially higher than those employed in the experiments of Adams et al. [2], namely, 10, 25, or 50 µg/L. As shown in Table 1, however, the initial PFOA concentration is set to 20×10^{-6} mol L^{-1} (80,280 µg/L), corresponding to the same molar concentration employed in the experiments of Stratton et al. [4].

The initial concentrations of both $S_2O_8{}^{2-}$ and H^+ determine the conditions governing the formation of reactive species, including sulfate radicals ($SO_4{}^{\bullet-}$) and hydrogen atoms (H). In principle, pH provides a measure of the hydronium ion concentration (H^+). As indicated in Table 1, when the pH varies from 1 to 5, the corresponding H^+ concentration ranges from 10^{-1} to 10^{-5} M (mol L^{-1}), respectively.

In the context of CO_2 reduction reactions, the influence of pH on the dynamics of CRN was discussed in detail in previous work [19]. Although the CRN system investigated here is different, the same mathematical treatment can be applied to PFAS degradation.

Regarding the initial $S_2O_8{}^{2-}$ concentration, a brief survey of the literature revealed the following reported values: 0.005–0.013 M (mol L^{-1}) [20], 0.005 M [21], and 0.05 M [12]. The concentrations explored in the computational experiments of the present work extend considerably beyond those typically employed in conventional chemical reactors. As shown in Table 1, the investigated $S_2O_8{}^{2-}$concentrations range from 0.005 to 500 M (mol L^{-1}), thereby allowing us to investigate the CRN dynamics over a substantially broader concentration range than that accessible under standard bench-scale reactor conditions.

II.c) Computational method

To investigate the temporal evolution of each dependent variable, the system of ordinary differential equations (ODEs) must be solved using a numerical integration method. In the present work, we chose the fourth-order Runge–Kutta method (RK4). Its implementation can be carried out using a compiled programming language, such as C++ or Fortran.

A numerical integration method discretizes the time variable (t), which is the variable we assign values. This means that discrete time values must be defined to calculate the corresponding values of the dependent variables. The time variable ranges from zero to t_f(final time), being the latter determined computationally through a trial-and-error procedure. Thus, the time domain is represented by a vector containing values incremented by the time step (Δt), $\{0,\ \Delta t,\ 2\Delta t,\ 3\Delta t,\ \cdots, i\cdot\Delta t,\ \ldots,\ t_f\}$, where i is a positive integer $\{1, 2, 3, \ldots\}$. To minimize numerical errors at each integration step, we set the time step (Δt) to approximately 10^{-7}s. Larger time steps tend to introduce significant errors in the calculated instantaneous reactant concentrations. The numerical solution for any free variable, $[v]$, defined by Equ. (12)–(17), can be expressed in the general form:

$$[v]_{inst} = [v]_0 + \left(\frac{d[v]}{dt}\right)_{inst} \Delta t \quad (19)$$

In Equ. (19), $[v]_0$ denotes the initial concentration of the variable $[v]_{inst}$, whereas the term $(d[v]/dt)_{inst}$represents the instantaneous rate of change obtained from the numerical integration of Equ. (12)–(17). The time variable, t, is defined by the discrete vector $\{0,\ \Delta t,\ 2\Delta t,\ 3\Delta t,\ \ldots,\ t_f\}$.

It is worth noting that the numerical integration method generates a vector of $d[v]/dt$ values, representing the instantaneous rates of change at successive time steps. Consequently, Equ. (19) describes the corresponding instantaneous concentration values, $[v]_{inst}$. To obtain the absolute concentration values throughout the integration period, the solution vector must be constructed recursively, as follows:

 © by the author(s) 2026, Layout by G-Labs

Parameter	Values	Unit	Ref.	meaning
k_1	7.1×10^8	L mol^{-1} s^{-1}	[10]	Rate constant of reaction 1
k_2	4.0×10^7	L $mol^{-1}s^{-1}$	[11]	Rate constant of reaction 2
k_3	1.2×10^{10}	L mol^{-1} s^{-1}	[11]	Rate constant of reaction 3
k_4	6.0×10^9	L mol^{-1} s^{-1}	[11]	Rate constant of reaction 4
k_5	2.3×10^{10}	L mol^{-1} s^{-1}	[11]	Rate constant of reaction 5
k_6	2.5×10^{10}	L mol^{-1} s^{-1}	[11]	Rate constant of reaction 6
k_7	1.0×10^{10}	L mol^{-1} s^{-1}	[16]	Rate constant of reaction 7
k_8	8.1×10^8	L mol^{-1} s^{-1}	[16]	Rate constant of reaction 8
k_9	1.2×10^6	L $mol^{-1}s^{-1}$	[16]	Rate constant of reaction 9
k_{10}	6.0×10^1	L $mol^{-1}s^{-1}$	[16]	Rate constant of reaction 10
k_{11}	2.5×10^7	L $mol^{-1}s^{-1}$	[22]	Rate constant of reaction 11
q_e	82.91×10^{-9}	mol s^{-1}	[8]	Rate of electron injection @ 8 mA
q_e	775.00×10^{-9}	mol s^{-1}	[23]	Rate of electron injection @ 75 mA
V	2.36×10^{-9}	L	[18]	Volume of the EPLI reactor
$[e]_0$	zero	mol L^{-1}		Initial concentration of hydrated electron
$[PFOA]_0$	2.0×10^5	mol L^{-1}	[4]	Initial concentration of PFOA
$[S_2O_8]_0$	0.005, 12.5, 50, 125, 500 and 1,500	mol L^{-1}	Fig 4	Initial concentration of peroxydisulfate
$[H^+]_0$	10^{-1}, 10^{-2}, 10^{-3}, 10^{-4}, 10^{-5} and $10^{-5.9}$ @ pH = {1, 2, 3, 4, 5 and 5.9}	mol L^{-1}	[19]	Initial concentration of hydrogen cation
$[H•]_0$	zero	mol L^{-1}		Initial concentration of hydrogen radical
$[R]_0$	zero	mol L^{-1}		Initial concentration of sulfate radical

Table 1: Parameters of the CRN used in the computational experiments.

 © by the author(s) 2026, Layout by G-Labs

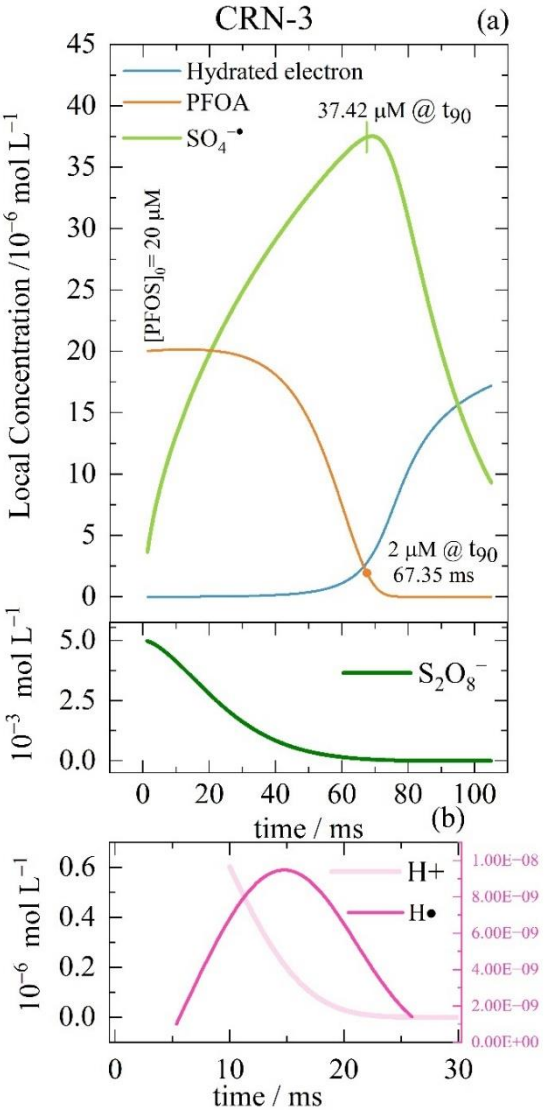


Figure 3. Local EPLI concentration of (a) hydrated electron, PFOA and Peroxydisulfate in a large time scale, and of (b) hydrogen ion and hydrogen radical in a short time scale. Numerical solution of CRN used parameter set shown in the Tab. 1, specifically q_e @ 8 mA, pH of 5.9, local reactor volume of 2.36 nL, 20 µM of initial PFOA concentration and 5 mM of initial $S_2O_8^{-}$concentration; finally, t_f of 0.1 seconds for plate (a) and 0.03 seconds for (b).

$$[v]_{n+1} = [v]_n + \left(\frac{d[v]}{dt}\right)_{n+1} \Delta t \qquad (20)$$

Consequently, the instantaneous concentration values, $[v]_{inst}$, are represented by the vector $\{[v]_0, [v]_{\Delta t}, [v]_{2\Delta t}, [v]_{3\Delta t}, \cdots, [v]_{t_f}\}$, whereas the absolute concentration values obtained through the recursive procedure described in Equ. (20) are represented by the vector $\{[v]_0, [v]_{n+1}, \cdots, [v]_N\}$, where N is the total number of integration steps.

We recall that SCILAB and MATLAB are primarily interpreted programming environments rather than compiled languages. Therefore, their numerical algorithms generally rely on built-in or external packages that implement specific numerical methods. However, it is not always clear which numerical integration method is implemented within a given package, such as the Euler or fourth-order Runge–Kutta (RK4) method.

In the present work, we chose to use Wolfram Mathematica because its user-friendly interface facilitated the implementation and execution of the computational experiments. However, since the specific numerical integration method employed by Mathematica's built-in syntax was not established, we independently implemented the RK4 method in C++ and compared the results with those obtained using Wolfram Mathematica. Both approaches yielded very good agreement, provided that the same integration time step was used in both implementations. Normally, the step $\Delta t = 10^{-9}$ yields low error.

III. Results and Discussion

III.a) CRN analysis – intrinsic mechanism of sulfate radical induced by the hydrated electrons

Fig. 3 shows the temporal evolution of the free variables of the CRN proposed in Fig. 2, whose model comprises the system of Equ. (12)–(17). The PFOA concentration continuously decreases due to the reaction described in Equ. (1), whereas the sulfate radical concentration increases markedly due to the reaction described in Equ. (4). The temporal evolution of the hydrated electron concentration is synchronized with the time required for the PFOA concentration to reach its minimum value. This behaviour occurs because both persulfate activation (generation of $SO_4^{\bullet-}$) and PFOA reduction consume hydrated electrons, which are the common reactant in both reactions. The synchrony between these processes is particularly evident at t_{90}, defined as the time required to achieve 90% abatement of the initial pollutant concentration. At t_{90} = 67.35 ms, PFOA concentration declines from 20 to 2 µM. Also, at t_{90}, $SO_4^{\bullet-}$concentration approaches its maximum value of approximately 37.42 µM.

The PFOA degradation shown in Fig. 3a is exclusively attributed to the action of hydrated electrons, i.e., the reductive degradation of PFOA

 © by the author(s) 2026, Layout by G-Labs

according to Equ. (1). Despite the simultaneous activation of persulfate, the CRN (chemical mechanism) proposed in this work does not account for subsequent reactions between the resulting sulfate radicals and PFOA or its degradation intermediates. Implementing a comprehensive chemical mechanism that includes all the reaction steps leading to the complete conversion of PFOA into CO_2 (mineralization) would require substantial mechanistic assumptions and speculation regarding the reaction pathways following radical formation. As discussed below, an alternative, albeit approximate, approach is to estimate the amount of perfluoroalkyl radicals ($C_8F_{14}O_2^{\bullet}$) that could potentially undergo complete oxidation by the sulfate radicals generated at the EPLI.

The degree of mineralization is estimated based on the complete conversion of one perfluoroalkyl radical into CO_2. For this purpose, Equ. (21) was balanced to describe the complete mineralization of a single perfluoroalkyl radical ($C_8F_{14}O_2^{\bullet}$). According to the stoichiometry of Equ. (21), fourteen sulfate radicals are required to fully convert one perfluoroalkyl radical into CO_2. Therefore, the maximum instantaneous sulfate radical concentration of 37.42 µM obtained in Fig. 3 corresponds to a theoretical mineralization capacity of 2.67 µM of perfluoroalkyl radicals (37.42 µM/14). Thus, under the operating conditions considered in Fig. 3, this amount of perfluoroalkyl radicals could potentially be fully mineralized into CO_2, in addition to the 90% PFOA abatement achieved at t_{90}.

$$C_8F_{14}O_2^{\bullet} + 14\,SO_4^{\bullet-} + 14\,H_2O \rightarrow 8\,CO_2 + 14\,HF + 14\,H^+ + 14\,SO_4^{2-} \quad (21)$$

In conclusion, the computational experiment shown in Fig. 3 predicts 90% PFOA abatement (18 µM/20 µM) and a theoretical mineralization degree of 13% (2.67 µM/20 µM). The abatement percentage is calculated from the difference between the initial PFOA concentration (20 µM) and its instantaneous concentration at t_{90} (2 µM). Similarly, the mineralization percentage is estimated from the maximum instantaneous sulfate radical concentration (37.42 µM), which corresponds to a theoretical capacity to mineralize 2.67 µM of perfluoroalkyl radicals, according to the stoichiometry of Equ. (21). This amount is normalized against the initial PFOA concentration (20 µM). Both calculations therefore rely on instantaneous concentrations obtained at t_{90} = 67.35 ms, rather than on cumulative reaction products explicitly quantified by the CRN. PFOA abatement is promoted by the reductive action of hydrated electrons, whereas the estimated mineralization capacity results from the oxidative action of sulfate radicals.

The locally generated aqueous hydrogen radicals (H•) are shown in Fig. 3b. However, similarly to the sulfate radicals, their subsequent interactions with PFOA are not explicitly included in the CRN presented in Fig. 2. Therefore, an alternative stoichiometric analysis, analogous to that performed for sulfate radicals, can be used to estimate their potential contribution to PFOA degradation. The maximum instantaneous H• concentration reaches 0.57 µM. According to the stoichiometry of the reaction presented in Equ. (11), one H• radical is required to reduce one PFOA molecule. Thus, the maximum H• concentration of 0.57 µM corresponds to a theoretical PFOA reduction capacity of 0.57 µM, representing less than 3% of the initial PFOA concentration (0.57 µM/20 µM). This contribution is negligible compared with the 90% PFOA abatement attributed to hydrated electron reduction. Therefore, under the conditions investigated in Fig. 3, hydrated electrons are the predominant species responsible for PFOA abatement, whereas the contribution of H• radicals is comparatively minor.

III.b) Optimizing radicals' production

To optimize radical production, or more specifically, the maximum instantaneous radical concentrations, the relevant experimental variables include the peroxydisulfate concentration, the H^+ concentration (pH), and the electrical current. The highest practical plasma current reported for DC plasma was observed in the study by Urabe et al. [23]. Therefore, we selected half of this value, corresponding to 75 mA, as the upper current limit for our computational experiments. Regarding pH, a value of 2 was selected as the lowest practical pH considered in this study, corresponding to the highest H^+ concentration investigated. These two parameters were used as operating benchmarks for the computational experiments presented in Fig 4. Fig. 4a and 4b show the temporal evolution of the hydrogen radical (H•) and sulfate radical ($SO_4^{\bullet-}$) concentrations, respectively. Fig. 4c summarizes the impact of increasing peroxydisulfate concentrations on the maximum instantaneous concentrations of both radicals.

 © by the author(s) 2026, Layout by G-Labs

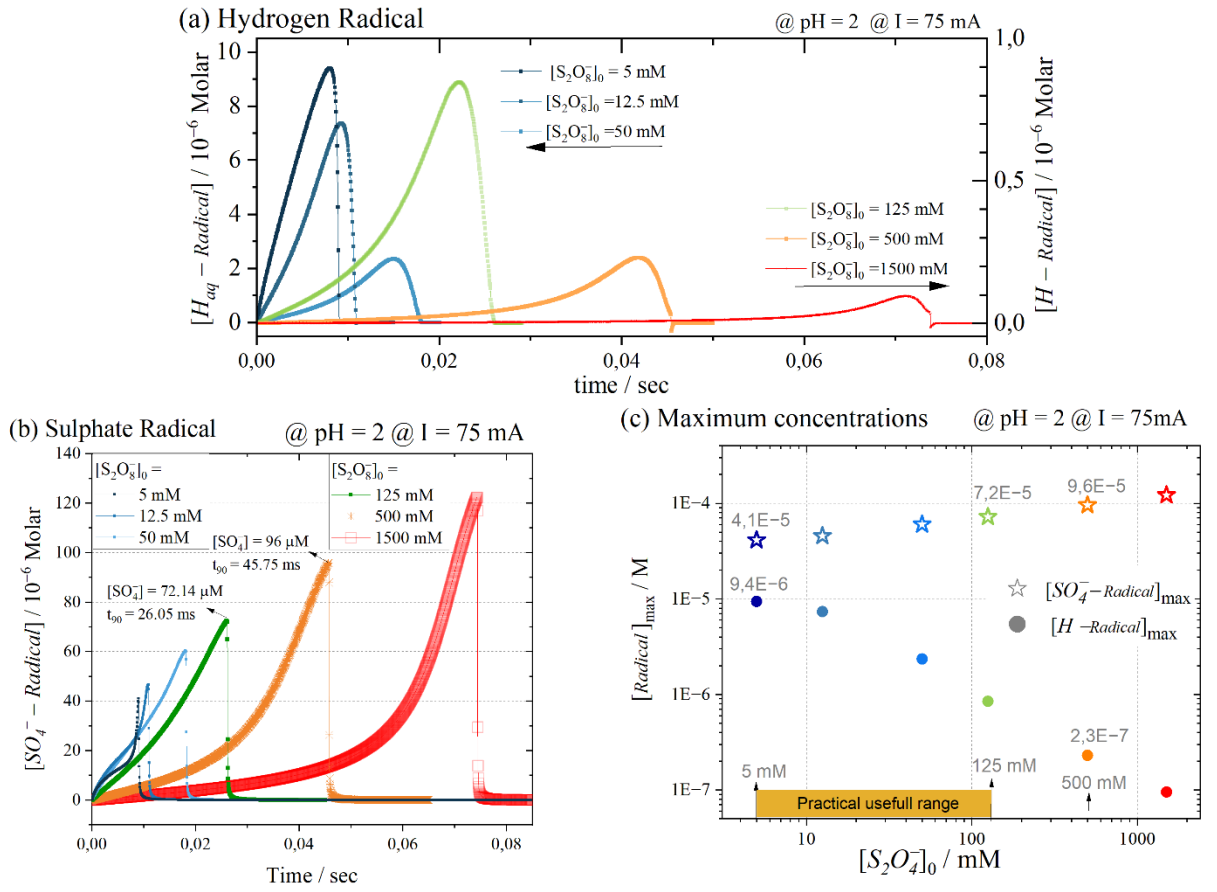


Figure 4. Time-resolved local concentration of (a) aqueous radical H, (b) sulphate radical, $\boldsymbol{SO_4^{\bullet-}}$, and (c) top concentration reached by the latter two for different initial concentration of sulphate radical precursors, $S_2O_8^-$. Numerical solution of CRN seeing in Fig. 2 used parameters from Table 1 specifically $\boldsymbol{q_e}$ for current of 75 mA, pH of 2, local reactor volume of 2.36 nL and 20 μM of initial PFOA concentrations.

The impact of electrical current and pH on the theoretical PFOA mineralization capacity is relatively modest. Considering a peroxydisulfate concentration of 5 mM in Fig. 4, the maximum instantaneous concentrations of $SO_4^{\bullet-}$ and H• reach 41.10 μM and 9.36 μM, respectively. Based on the stoichiometry of Equ. (21), the maximum sulfate radical concentration theoretically allows for the mineralization of 2.94 μM of perfluoroalkyl radicals (41.10 μM/14). In other words, the optimized electrical current and pH conditions yield a theoretical PFOA mineralization capacity of 14.67% (2.94 μM/20 μM). In our view, the optimized current produces only a modest improvement in the theoretical mineralization capacity, increasing it from approximately 13% at 8 mA to 14.67% at 75 mA. Regarding the maximum H• concentration, its value of 9.36 μM corresponds to a theoretical PFOA reduction capacity of 9.36 μM, representing 46.80% of the initial PFOA concentration (9.36 μM/20 μM), according to the stoichiometry of Equ. (11). Therefore, increasing the electrical current and decreasing the pH are effective strategies for increasing the maximum instantaneous H• concentration and, consequently, the theoretical PFOA reduction capacity. However, these operating parameters have only a modest impact on the maximum instantaneous $SO_4^{\bullet-}$ concentration and, consequently, on the estimated mineralization capacity.

The effect of peroxydisulfate concentration ($S_2O_8^{2-}$) as an optimization parameter for PFOA mineralization is analyzed next. Interestingly, increasing the maximum instantaneous $SO_4^{\bullet-}$ concentration also decreases the EPLI-induced H• concentration, as shown in Fig. 4c. Increasing the $S_2O_8^{2-}$ concentration from 5 to 125 mM leads to a substantial improvement in the theoretical mineralization capacity. Within this concentration range, the maximum instantaneous $SO_4^{\bullet-}$ concentration increases from 41.10 to 72 μM. The latter value corresponds to a theoretical capacity to mineralize 5.14 μM of perfluoroalkyl radicals (72 μM/14) instantaneously, representing 25.7% of the initial PFOA concentration (5 μM/20 μM). Thus, increasing the $S_2O_8^{2-}$ concentration from 5 to 125 mM increases the estimated PFOA

 © by the author(s) 2026, Layout by G-Labs

mineralization capacity from approximately 13% to 25%. We suggest the range from 5 to 125 mM of $S_2O_8^{2-}$ as a practical value for an EPLI-industrial reactor.

This study proposes a novel strategy toward the simultaneous abatement and mineralization of PFOA and other PFAS by designing a coupled treatment system that does not rely on separate reductive and oxidative treatment stages. In the process proposed by Zhang et al. [24], for example, two separate stages are employed: a pretreatment step in which PFOA is reduced by hydrated electrons, followed by a post-treatment oxidation step using a boron-doped diamond (BDD) anode. Conversely, EPLI-based technology is capable of generating both reductive and oxidative species within the same reaction volume and timescale. The present work demonstrates the simultaneous formation of hydrated electrons (e_{aq}^-), sulfate radicals ($SO_4^{\bullet-}$), and hydrogen radicals (H•) within a single EPLI reactor. Furthermore, the industrial scale-up of EPLI technology could be relatively straightforward, as it would primarily involve increasing the number of plasma tip/water-surface interfaces.

IV. Conclusion

This work presents a chemical dynamical model to elucidate the activation and reactivity of sulfate radicals ($SO_4^{\bullet-}$) at the electrified plasma–liquid interface (EPLI). In general, EPLI-induced hydrated electrons (e_{aq}^-) promote PFOA degradation with low Faradaic efficiency, meaning that most of the hydrated electrons generated at the EPLI are consumed by water splitting, thereby producing gaseous hydrogen (H_2), as described in Equ. (2). In this work, the use of peroxydisulfate ($S_2O_8^{2-}$) in the aqueous phase is proposed as a strategy to activate sulfate radicals ($SO_4^{\bullet-}$), according to Equ. (4). This approach provides a means of redirecting hydrated electrons toward the generation of additional reactive species, potentially increasing the Faradaic efficiency of the process while reducing hydrogen production.

Considering pH = 5.9, a constant current of 8 mA, and an initial $S_2O_8^{2-}$ concentration of 5 mM, our computational experiments revealed that EPLI-induced hydrated electrons enable the formation of both $SO_4^{\bullet-}$ and $H^{\bullet}$ radicals in the aqueous phase. Based on their maximum instantaneous concentrations, these radicals correspond to theoretical instantaneous capacities for mineralizing 13% and reducing less than 3% of the initial PFOA concentration, respectively. These contributions are estimated alongside 90% PFOA abatement through direct reduction by hydrated electrons.

Finally, we investigated three operating parameters—electrical current, pH, and $S_2O_8^{2-}$ concentration—with regard to their potential to enhance PFOA mineralization. The combined effects of electrical current and pH had only a modest impact on the theoretical PFOA mineralization capacity through $SO_4^{\bullet-}$ oxidation. However, these parameters significantly enhanced the theoretical contribution of aqueous H• radical reduction to PFOA abatement, increasing its estimated contribution from less than 3% to 46.8%. In contrast, increasing the $S_2O_8^{2-}$ concentration proved effective in enhancing the theoretical instantaneous PFOA mineralization capacity from 13% to 25%. These values represent a potentially relevant contribution when compared with current mineralization benchmarks reported for various water treatment reactors. Specially because they are instantaneous mineralization degrees measured at the top radical concentration. If the hole treatment time (t_{90} = 67.35 ms or 26.05 ms, respectively) were considered, the integrated mineralization degree could reach one hundred percentage.

Last but not least, we evaluate the practical limitations of the present work. In a practical EPLI reactor, the primary species responsible for PFAS degradation is potentially the plasma-phase H radical, rather than hydrated electrons, as previously argued by us [9]. Nevertheless, the present work proposes a chemical reaction network (CRN) that considers hydrated electrons exclusively as the reductive species. This choice was motivated by our intention to demonstrate the potential of EPLI reactors to generate a broad spectrum of radicals in both the liquid and plasma phases, as well as their ability to steer pollutant degradation towards mineralization by varying the overall experimental parameters.

In future work, we hope that the advanced oxidation and reduction processes community will undertake experimental validation of either or, ideally, both of these contributions. Further theoretical developments will only be meaningful if guided and supported by experimental evidence.

 © by the author(s) 2026, Layout by G-Labs

AI statement

The final version of this manuscript was submitted to ChatGPT for grammar mistake identification. All AI-generated content was carefully reviewed, verified, and edited by the authors, who accept full responsibility for the final published work.

Competing financial interest statement

The authors declare that they have no known competing financial interests or personal relationships that could have appeared to influence the work reported in this paper.

References

[1] D. Alam, S. Lee, J. Hong, D.F. Fletcher, X. Liu, et al., "Influence of bubble size on perfluorooctanesulfonic acid degradation in a pilot scale non-thermal plasma treatment reactor," *Chem. Engineering J.*, vol. 489, 2024. DOI: 10.1016/j.cej.2024.151349

[2] D. Alam, S. Lee, J. Hong, D.F. Fletcher, D. McClure, et al., "Experimental investigations of Per- and Poly-fluoroalkyl substances (PFAS) degradation by non-thermal plasma in aqueous solutions," *J. of Environ. Chem. Engineering*, vol. 11, 2023. DOI: 10.1016/j.jece.2023.111588

[3] R.K. Singh, N. Multari, C. Nau-Hix, R.H. Anderson, S.D. Richardson, et al., "Rapid Removal of Poly- and Perfluorinated Compounds from Investigation-Derived Waste (IDW) in a Pilot-Scale Plasma Reactor," *Environ. Sci. Technol.,* vol. 53, 2019. DOI:

[4] G.R. Stratton, F. Dai, C.L. Bellona, T.M. Holsen, E.R. Dickenson, S. Mededovic Thagard, "Plasma-Based Water Treatment: Efficient Transformation of Perfluoroalkyl Substances in Prepared Solutions and Contaminated Groundwater," *Environ. Sci. Technol.,* vol. 51 2017. DOI: 10.1021/acs.est.6b04215

[5] R.K. Singh, S. Fernando, S.F. Baygi, N. Multari, S.M. Thagard, T.M. Holsen, "Breakdown Products from Perfluorinated Alkyl Substances (PFAS) Degradation in a Plasma-Based Water Treatment Process," *Environ Sci Technol.,* vol. 53, 2019. DOI: 10.1021/acs.est.8b07031

[6] C. Nau-Hix, N. Multari, R.K. Singh, S. Richardson, P. Kulkarni, R.H. Anderson, et al., "Field Demonstration of a Pilot-Scale Plasma Reactor for the Rapid Removal of Poly- and Perfluoroalkyl Substances in Groundwater," *ACS ES&T Water,* vol. 1, 2021. DOI: 10.1021/acsestwater.0c00170

[7] P. Rumbach, D.M. Bartels, R.M. Sankaran, D.B. Go, "The solvation of electrons by an atmospheric-pressure plasma," *Nature Communications*, vol. 6, 2015. DOI: 10.1038/ncomms8248

[8] J.R. Toth, R. Hawtof, D. Matthiesen, J.N. Renner, R.M. Sankaran, "On the Non-Faradaic Hydrogen Gas Evolution from Electrolytic Reactions at the Interface of a Cathodic Atmospheric-Pressure Microplasma and Liquid Water Surface," *J. of The Electrochem. Soc.*, vol. 167, 2020. DOI: 10.1149/1945-7111/aba15c

[9] A. Mota-Lima, "H-driven degradation of PFAS in the gas/liquid interface using electrochemistry configuration of cold plasma," *J. of Technol. and Space Plasmas*, vol. 6, 2025. DOI: 10.1149/1945-7111/aba15c

[10] W.A. Maza, V.M. Breslin, J.C. Owrutsky, B.B. Pate, A. Epshteyn, "Nanosecond Transient Absorption of Hydrated Electrons and Reduction of Linear Perfluoroalkyl Acids and Sulfonates," *Environ. Science & Technology Letters*, vol. 8, 2021. DOI: 10.1021/acs.estlett.1c00383

[11] G.V. Buxton, C.L. Greenstock, W.P. Helman, A.B. Ross, "Critical Review of rate constants for reactions of hydrated electrons, hydrogen atoms and hydroxyl radicals (·OH/·O− in Aqueous Solution," *J. of Phys. and Chem. Reference Data*, vol. 17, 1988. DOI: 10.1063/1.555805

[12] H. Hori, Y. Nagaoka, M. Murayama, S. Kutsuna, "Efficient Decomposition of Perfluorocarboxylic Acids and Alternative Fluorochemical Surfactants in Hot Water," *Environ. Science & Technology*, vol. 42, 2008. DOI: 10.1021/es800832p

[13] P.M. Dombrowski, P. Kakarla, W. Caldicott, Y. Chin, V. Sadeghi, et al., "Technology review and evaluation of different chemical oxidation conditions on treatability of PFAS," *Remediation J.*, vol. 28, 2018. DOI: 10.1002/rem.21555

[14] H.V. Lutze, J. Brekenfeld, S. Naumov, C. von Sonntag, T.C. Schmidt, "Degradation of perfluorinated compounds by sulfate radicals - New mechanistic aspects and

 © by the author(s) 2026, Layout by G-Labs

economical considerations," *Water Res.*, vol. 129, 2018.
DOI: 10.1016/j.watres.2017.10.067

[15] C. Zhang, T. Tang, D.R.U. Knappe, "Oxidation of Per- and Polyfluoroalkyl Ether Acids and Other Per- and Polyfluoroalkyl Substances by Sulfate and Hydroxyl Radicals: Kinetic Insights from Experiments and Models," *Environ. Science & Technology*, vol. 57, 2023. DOI: 10.1021/acs.est.3c00947

[16] P. Neta, R.E. Huie, A.B. Ross, "Rate Constants for Reactions of Inorganic Radicals in Aqueous Solution," *J. of Phys. and Chem. Reference Data*, vol. 17, 1988.
DOI: 10.1063/1.555808

[17] A. Mota-Lima, J.F. do Nascimento, O. Chiavone-Filho, C.A.O. Nascimento, "Electrosynthesis via Plasma Electrochemistry: Generalist Dynamical Model to Explain Hydrogen Production Induced by a Discharge over Water," *The J. of Phys. Chem. C*, vol. 123, 2019.
DOI: 10.1021/acs.jpcc.9b04777

[18] I. Gonçalves, J. Barauna, F. Cunha-Filho, O. Chiavone-Filho, J. Vitoriano, et al., "Reduction of Aqueous Ag+ Steered by Electrochemical Plasma: Connecting the Bulk pH Variation with the Reaction Pathways for Hydrated Electrons," *J. of the Brazilian Chem. Soc.*, vol. 30, 2019. DOI: 10.21577/0103-5053.20190020

[19] A. Mota-Lima, "Ratio Oxalate to Formate Tuned by pH During CO2 Reduction Driven by Solvated Electron at the Electrified Plasma/Liquid Interface," *Electrocatalysis*, vol. 11, 2020. DOI: 10.1007/s12678-020-00620-z

[20] E.L. Foletto, J. A. B. de Souza, O. Chiavone-Filho, "Oxidação de poluente aromático via persulfato catalisado por material ferroso suportado em biochar derivado de C. procera," *23º Congresso Brasileiro de catálise Sociedade Brasileira de catálise*, Vol. 1, 2025.
https://submissao.cbcat.sbcat.org/index.php/23CBCAT/article/view/36

[21] C. Zhang, T. Tang, D.R.U. Knappe, "Oxidation of Per- and Polyfluoroalkyl Ether Acids and Other Per- and Polyfluoroalkyl Substances by Sulfate and Hydroxyl Radicals: Kinetic Insights from Experiments and Models," *Environ. Science & Technology*, vol. 57, 2023. DOI: 10.1021/acs.est.3c00947

[22] T. Szreder, J. Kisala, A. Bojanowska-Czajka, M. Kasperkowiak, D. Pogocki, et al., "High energy radiation - Induced cooperative reductive/oxidative mechanism of perfluorooctanoate anion (PFOA) decomposition in aqueous solution," *Chemosphere,* vol. 295, 2022. DOI: 10.1016/j.chemosphere.2022.133920

[23] K. Urabe, N. Shirai, K. Tomita, T. Akiyama, T. Murakami, "Diagnostics of atmospheric-pressure pulsed-dc discharge with metal and liquid anodes by multiple laser-aided methods," *Plasma Sources Sci. Technol.*, vol. 25, 2016.
DOI: 10.1088/0963-0252/25/4/045004

[24] W. Zhang, Q. Long, G. Li, Z. Ning, L. Lu, "Electrochemical oxidation coupled with hydrated electron reduction in ultraviolet (UV)-sulfite system for complete defluorination and mineralization of Perfluorooctanoic Acid (PFOA)," *J. of Water Process Engineering*, vol. 53, 2023. DOI: 10.1016/j.jwpe.2023.103836

Open Access. This article is licensed under a Creative Commons Attribution 4.0 International License, which permits use, sharing, adaptation, distribution and reproduction in any medium or format, as long as you give appropriate credit to the original author(s) and the source, provide a link to the Creative Commons license, and indicate if changes were made. The images or other third party material in this article are included in the article s Creative Commons license, unless indicated otherwise in a credit line to the material. If material is not included in the article's Creative Commons license and your intended use is not permitted by statutory regulation or exceeds the permitted use, you will need to obtain permission directly from the copyright holder. To view a copy of this license, visit: http://creativecommons.org/licenses/by/4.0/.